Bifurcations in Poiseuille flow and wall turbulence

Javier Jimenez
School of Aeronautics, Universidad Politécnica
Pl. Cardenal Cisneros 3, 28040 Madrid, Spain
and IBM Madrid Scientific Centre

The fully nonlinear stage of two dimensional Poiseuille flow undergoes a limit cycle bifurcation, whose detailed mechanism is studied using full numerical simulations of simple, spatially periodic cases. It is also shown that this mechanism, a periodic ejection from the wall layer, underlies the production of turbulence in more complicated two dimensional situations. Vorticity ejections are also present in the sublayer of three dimensional channels. Their behaviour is studied briefly in three dimensional simulations. A simplified model system is then proposed and studied. There are important differences between the two ejections mechanisms, due to the presence of three dimensional vorticity.

It is generally accepted that turbulence, and, in particular, wall turbulence, is a three dimensional phenomenon in which processes such as hairpin eddies and vortex stretching play important roles. It has also been shown recently that transition to turbulence in wall bounded flows is intrinsically three dimensional, even if linear stability theory predicts that two dimensional disturbances are unstable at lower Reynolds numbers than their three dimensional counterparts. It appears that these disturbances are indeed the first ones to grow, but that, as soon as their amplitude is finite, they become themselves unstable to much faster three dimensional secondary instabilities, that quickly become dominant, and lead to turbulent breakdown. As such, the original two dimensional disturbances are never observed in their full amplitude, nonlinearly saturated, state. The first part of this paper, however, deals with the behaviour of precisely those nonlinear two dimensional waves in channel flows. We will show that it is possible to construct, computationally, statistically stationary and strictly two dimensional flows with properties such as chaotic behaviour, ejections, large scale intermittency, and quasi periodic bursting, all of which are observed in fully turbulent three dimensional flows. As such, and even if the range of behaviours described in this part of the paper goes from the laminar to the chaotic, it should not be considered as a study of turbulent transition in channels, but as a model for fully developed turbulent channel flow. A model that has been so severely truncated in the spanwise direction that it is actually two dimensional.

Two dimensional turbulence has been studied often, even if it is observed experimentally only under very special circumstances. There are several reasons for that, of which perhaps the most important is that it provides a simplified situation in which to study mechanisms that may be relevant to the three dimensional case. Two dimensional flows are much easier to compute and, above all, much easier to observe than three dimensional ones, and the mechanisms that act in them can generally be analysed rather fully. The understanding gained from these analyses can sometimes be carried into three dimensions, even if only as an indication of which features are intrinsically three dimensional, and which ones are not.

The question of three dimensionality is taken up in the next two sections of the paper, which analyse the flow field in three dimensional simulations of turbulent channels. First we deal with a simulation of a very wide channel, that can be considered a natural flow without constrains. It will be found that the mechanisms in the sublayer have many features in common with those found in the two dimensional case, but a better understanding of the details will have to wait until we discuss, in the next section, the flow in a simplified model channel that has been made periodic along the span with a wavelength of the order of the streak spacing in the sublayer. The result will be a tentative model for the events in the wall region, including the effect of longitudinal vorticity.

Spatially periodic Poiseuille flow is a good system in which to study self sustaining turbulence. Above a critical Reynolds number ($Re_Q \approx 5772$), it becomes linearly unstable and develops finite amplitude two dimensional motions which eventually saturate (Herbert, 1976) to a uniform equilibrium wavetrain. This new state is subcritical, and can be continued at finite amplitudes to Reynolds numbers that are lower than the linear stability threshold. This has led to the hope that these equilibrium wavetrains might explain the observed existence of real (three dimensional) turbulence at subcritical Reynolds numbers. This does not seem to be true. The limit for two dimensional equilibrium wavetrains is about $Re_Q = 2500$, while three dimensional turbulence has been observed down to $Re_Q \simeq 1500$. Moreover, the uniform wavetrain appears to be always unstable. At high Reynolds numbers it suffers a new bifurcation into a limit cycle, resulting in a periodic ejection of vorticity from the wall into the core of the channel (Jiménez, 1987). At all Reynolds numbers, the uniform wavetrain is also unstable to slow modulations in amplitude, leading to the appearance of isolated structures similar to turbulent "puffs", "slugs" and other features observed in pipe flow. In these new states, the limit cycle, observed in the uniform wavetrains at high Reynolds numbers, reappears at much lower ones, and the process leads directly to chaotic flows through an intermittency transition (Jiménez, 1988b).

Still, it has been shown repeatedly that two dimensional channel flows, even chaotic ones, are too organised to represent adequately real three dimensional turbulence, and that properties such as wall drag and turbulent intensities are lower than they should be (Rozhdestvensky & Simakin, 1984). Moreover, it is well known that besides the instabilities mentioned above, the nonlinear two dimensional wavetrains are unstable to a much stronger three dimensional instability that leads quickly to breakdown (Orszag & Patera, 1983). Still, our method will be to study simple models, in part for their own sake, and in part in the hope that similar phenomena hide similar mechanisms, and that something of what we learn in two dimensions and in narrow periodic channels will carry into the less constrained real flows.

The two dimensional channel

Poiseuille flow is initially established between two infinite parallel plates at $y = \pm h$, with a parabolic laminar equilibrium velocity profile. It is governed by the 2D vorticity equation

$$\omega_t + \psi_y \omega_x - \psi_x \omega_y = Re^{-1} \nabla^2 \omega, \tag{1}$$

where ψ is a stream function, and

$$\omega = \nabla^2 \psi \tag{2}$$

is the vorticity. Throughout this paper we will use units such that the half channel width is $h = 1$, and the volume flux per unit span, which we will be assume to be independent of time, is $Q = 4/3$. In these units, the initial parabolic velocity profile is $U(y) = 1 - y^2$, and a natural Reynolds number is $Re_Q = 3Q/4\nu$ Eqs. (1-2) form an initial value problem that is integrated directly, without any turbulence modelling, using a pseudo-spectral method, that is described in (Jiménez, 1988a). The main simplification, besides that of two-dimensional flow, is that the equations are solved in a finite computational box, of streamwise length $2\pi/\alpha$, where α is a wavenumber, and that the flow is assumed to extend periodically outside that box.

As mentioned above, at low Reynolds number, the parabolic profile is stable, and a small arbitrary perturbation dies. Above $Re_Q = 5772$ ($\alpha = 1.02$), a linear instability appears and initial perturbations grow until they reach a saturated nonlinear state which, because of the constrain of spatial periodicity implicit in the boundary conditions, is a uniform train of nonlinear waves that, by analogy to the linear case, will be called Tollmien Schlichting (T-S) waves. These equilibrium wavetrains form an "upper sheet" of solutions, parameterised by Re_Q and by the wavenumber α, that has been mapped in (Zahn *et al.*, 1974, Herbert, 1976) and extends in a narrow range of wavenumbers ($\alpha \simeq 0.9$-1.7, depending on Re_Q), and down to a subcritical $Re_Q = 2500$. At low Reynolds numbers, the solutions in this surface are not only stable, but attracting, at least in the space of periodic functions with period $2\pi/\alpha$, and can be reached by perturbing the laminar flow with sufficiently strong *finite amplitude* initial perturbations.

The general character of these equilibrium wavetrains can be seen in Fig. 1. The vorticity distribution in the core of the channel is dominated by two large vortices of alternating sign, which are just a deformation of the original laminar vorticity distribution. These two vortices induce strong secondary vorticity peaks at the walls, to accommodate the no-slip condition. In the units defined above, the vorticity profile of the initial laminar flow is $\omega = -2y$, and attains it maximum value, $\omega = 2$, at the lower wall.

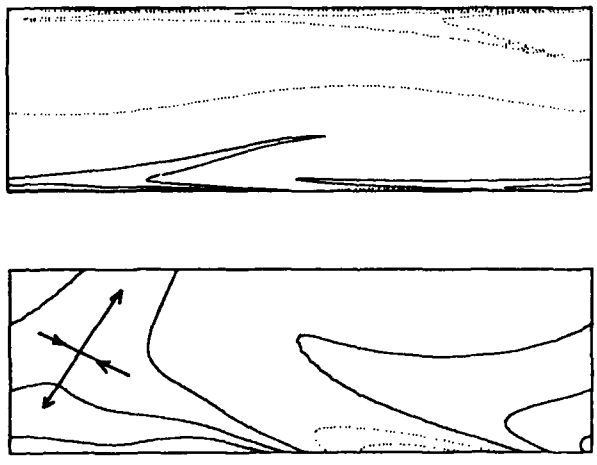

FIG. 1 Vorticity map of an equilibrium nonlinear periodic Tollmien Schlichting wave in a two dimensional channel. Vorticity isolines are: 0, ±1.4, ±2.8, ±4.2; dotted lines are zero or negative. $Re_Q = 5000$, $\alpha = 1.0$. Top map is full channel. Bottom is a blow-up of the wall region below $y/y_{wall} = 0.2$.

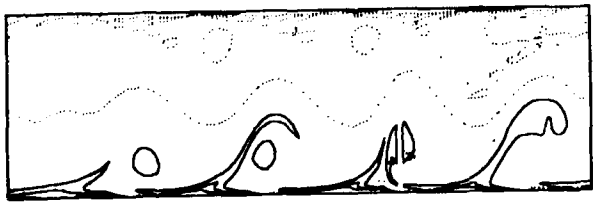

FIG. 4 Vorticity map of an chaotic wave train in a two dimensional channel. Vorticity isolines same as Fig. 1 $Re_Q = 7000$, $\alpha = 0.25$.

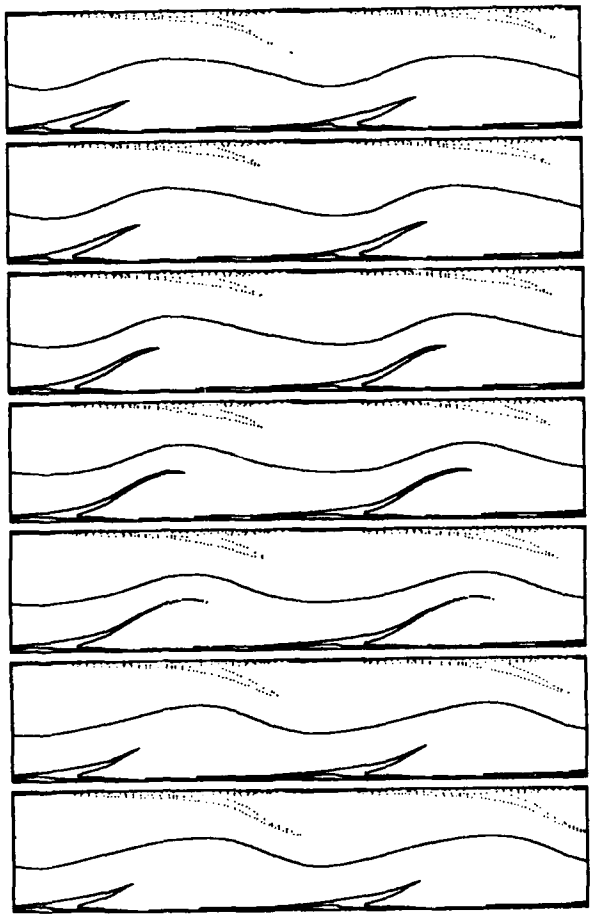

FIG. 2 Vorticity maps of a bursting two dimensional flow. Time is from top to bottom and axes move with the average perturbation. Isolines are: 0, ±1.5, ±3, ±5, ±7; dotted lines are negative. $Re_Q = 7000$, $\alpha = 1.0$. Time between frames, 1.6. Each plot represents two identical computational boxes.

where it fixes the wall shear stress and the pressure drop in the channel. The average wall vorticity of the nonlinear wavetrains is somewhat higher, ($\bar{\omega} = 2.2$ to 4.9 at $Re_Q = 7000$, depending on the wavenumber) but is the result of averaging between positive and negative vorticity peaks at the same wall whose characteristic value is $\omega_{peak} = \pm$ 6-15 (Fig. 1-b). For comparison, the average wall vorticity in a fully turbulent three dimensional channel, at $Re_Q = 7000$, is $\bar{\omega}_z = 11.5$ (Dean, 1978).

The combined effect of the large vortices in the core of the channel and the secondary vortices at the wall is to create transversal velocities which, in the proper frame of reference, generate a stagnation saddle point close to each wall (Fig. 1). Along the unstable directions from these saddles, vorticity from the wall layer leaks into the core and feeds the large diffuse vortices in that region. At low Reynolds number, this situation is stable, and the whole arrangement moves with a convection celerity $U_c = 0.40$-0.45, with a weak dependence on Re_Q. The core flow is essentially inviscid, and viscous effects are limited to a thin wall layer.

A wall shear velocity can be defined as, $u_\tau = (\bar{\omega}/Re_Q)^{1/2}$, and the corresponding expression for distance in wall units is $y^+ = (\bar{\omega} Re_Q)^{1/2} y$. In these units the thickness of the wall layer is of the order of 10, which is comparable to the one in full turbulent, three dimensional situations, and the convection celerity is $U_c^+ \simeq 22$, which corresponds to the average velocity of the flow at $y - y_{wall} \simeq .25$, or $y^+ \simeq 30$. As we will see in the next sections, this last value is too high when compared to three dimensional flows.

At Reynolds numbers above $Re_Q \simeq 5500$, this situation becomes itself unstable. At lower Re_Q, the vorticity of the separated shear layers is diffused by viscosity and blends steadily into the extended vortices in the channel core. As the Reynolds number increases, viscous diffusion is no longer sufficient and the shear layers become unsteady, feeding discrete blobs of vorticity into the channel. These blobs are convected along the centre of the channel at a faster velocity than the celerity of the T-S waves, and induce their own secondary vorticity perturbations on the walls. The result is a new system of wall vortices that interacts with the original one, producing periodic "bursts" of the separated shear layers. These bursts, in turn, generate the vorticity blobs that feed the instability, with a period around $T = 13$. At higher Reynolds numbers ($Re_Q \simeq 9100$) this simple limit cycle complicates into a torus with two discrete frequencies, and there is some evidence that, at still high Re_Q, it degenerates into temporal chaos.

Fig. 2 shows one "burst" of the separated layer at the lower wall. The frame of reference in this figure has been adjusted to move with the average perturbation, and the limit cycle appears as a simple extension and shrinking of the vortex sheet. Note that in this figure, as in the next one, we have represented two identical wavelengths of the simulation to aid in the interpretation as the structures move across the boundary of the computational box. Both walls burst alternatively, half a period apart. When the vorticity field is averaged over a whole period of the limit cycle, in axes fixed to the perturbation, the result is a structure looking a lot like the low Reynolds number flow field in Fig. 1. Fig. 3 shows the result of subtracting this averaged field from the actual vorticity distributions at different moments of the limit cycle, and represents the unsteady part of the flow. The part of this figure displaying the whole channel shows how the vortex blobs are convected along the channel centre, while the blow-up of the wall

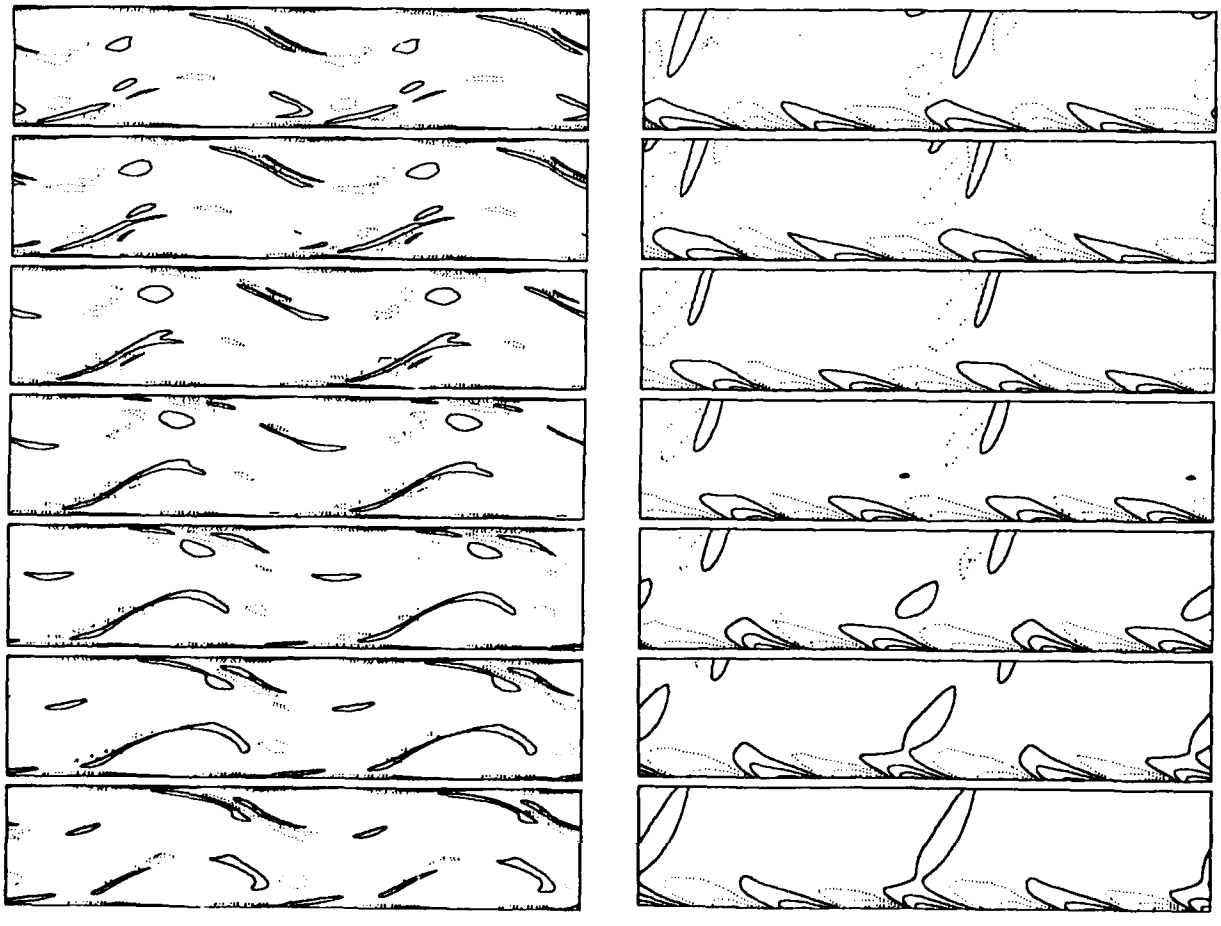

FIG. 3 Unsteady vorticity maps of the flow in Fig. 2. See text for explanation. Isolines are: ± 0.125, ± 0.5, ± 1, ± 1.5; dotted lines are negative. **Left:** Full channel. **Right:** Blow-up of wall layer below $y - y_{wall} = 0.2$.

region shows the system of secondary vortices. This alternating vortex train carries with it a sequence of updrafts and downdrafts that periodically reinforce or weaken the stagnation flow responsible for the separated layers, and they form the engine that drives the unsteady part the ejections.

This feedback process is not restricted to spatially periodic flows. When the periodicity restriction is relaxed by running the simulation in longer boxes containing several primary wavelengths $x \ll 1$, the uniform wavetrain becomes unstable to spatial modulations of the amplitude, and, at relatively low Reynolds numbers ($Re_Q > 6000$), becomes disorganised and chaotic (Jiménez, 1988b). Even in this case, the structure of each wavelength is essentially the same as in the periodic wavetrains, although their amplitudes and phases are now disorganised. From the study of movies of these flows, it is seen that the basic mechanism for the variability of the ejections is the same as in the limit cycle: vorticity ejected from one wave approaches the opposite wall and generates an induced wall vortex that modulates the next ejection. Therefore, at least in this simple two dimensional flow, the mechanism of variability and turbulence seem to be the modulation of wall ejections by a feedback from the outer part of the flow. In the next two sections we will inquire whether a similar mechanism can be found in three dimensional flows.

Three dimensional channels

As mentioned in the introduction, it has long been recognised that the structure of wall turbulence in boundary layers and channels is three-dimensional. A generally accepted picture is that blobs of low velocity fluid are ejected from the wall layer and interact with the mean shear to produce what can probably be described as horseshoe vortices (see e.g., Cantwell, 1981). The mechanism that triggers the initial ejection is, however, not understood, and there are indications that the processes controlling the behaviour of the viscous sublayer, where these ejections originate, are different from those active in the outer parts of the boundary layer.

We have seen in the previous section that a similar ejection process occurs in two dimensional channels, and that, in that case, it can be understood in terms of strong shear layers that originate at the wall and extend into the core. The way in which (spanwise) vorticity is injected into the core flow is crucial in fixing the wall shear stress and the pressure drop in the channel. In fact, the stress at the wall is equal to the viscous flux of vorticity per unit area away from the wall $Re^{-1}\partial\omega_z/\partial y$ and, since the total vorticity flux across planes parallel to the wall is independent of the location across the channel, the viscous vorticity transport of the wall layer has to be substituted by convective fluxes as we look farther into the core flow. These fluxes are just a different way of understanding the Reynolds stresses, and are implemented by the shear layers which are, therefore, the ultimate carriers of wall friction. Since we have seen that the friction coefficients are higher in three dimensional channels than in two dimensional ones, an equivalent ejection mechanism has to exist in three dimensions.

In fact, it was shown in (Jiménez *et al.*, 1988) that the sublayer of three dimensional turbulent channels is dominated by thin, and narrow, shear layers of high ω_z, which protrude into the core flow. They were observed using a short time series of flow fields extracted from the numerical simulation described in (Kim, Moin & Moser, 1987, referred from now on as KMM). This is a fully resolved numerical simulation, at $Re_Q = 4200$, of a channel which is 4π periodic in the x direction, and $4\pi/3$ periodic in the z direction. It was shown in (KMM) that its statistical properties are in good agreement with those of experimental flows, and we will consider it here as a "natural" turbulent channel. A cross section through one of the ω_z ejections is shown in Fig. 5.

There are some important differences between these structures and those in the 2-D calculations. To begin with, the "wavelength" seems to be shorter, with an average streamwise separation between consecutive features $x \simeq 1$-3 (in wall units, $x^+ \simeq 200$-500), while the 2-D nonlinear T-S waves can only exist, as equilibrium solutions, for wavelengths in a range $x \simeq 4$-6.5. Also, the layers in the three dimensional channel penetrate less into the core flow, appearing to level off at a distance of $y \simeq 0.2$, ($y^+ \simeq 35$) away from the wall, while the 2-D solutions extend all the way to the channel centre line. On the other hand, there is some evidence, in the 3-D flow, of weaker layers that do extend deeper into the core.

The main difference, however, is that the shear layers in the natural channel are three dimensional structures, with a spanwise extent of no more than $z \simeq 0.3$, or about 55 wall units, at $y^+ = 6$ ($z \simeq 0.4$ at the wall). They appear to be rooted at the wall in elliptical "hot" spots in which ω_z is at least 25% higher than its average wall value, and they extend into the channel with typical ejection angles of a few degrees. The "hot spots" can be used to detect and count the protruding layers and to follow their motion. They move with a convection celerity $U_c = 0.44$, which is in surprisingly good agreement with the celerity of the 2-D nonlinear waves. Although the significance of this agreement is not clear, this celerity corresponds to the average flow velocity at $y^+ \simeq 10$, which is still well inside the wall layer, suggesting that the spots and the layers are structures linked mainly to that region.

When the "hot spots" are followed into the flow in the form of three dimensional iso-surfaces of z-vorticity, they form a "forest" of leaning curving "necks" that covers much of the wall (Fig. 6). It is possible to follow the evolution of these structures as they move, and some of them were followed for fairly long periods, long enough for the structure to move several channel half widths. In the course of their life they reproduce, giving origin to new structures, and we were able to observe several of these reproduction

FIG. 5 Vorticity (ω_z) map of an x-y section of ejection structures in the KMM channel. Dotted lines: $\omega_z = -1.1$ and 0; dashed: 1.1 and 2.2; solid: 3.2 to 17.3. Average vorticity at wall: $\bar{\omega}_z = 7.7$. Each horizontal tick mark represents one half channel width ($x^+ = 180$), each vertical one, $y^+ = 17.5$. (From Jiménez *et al.*, 1988).

processes. First, the structure stretches, as its top is carried forward by the faster velocities far from the wall, and develops a small blob of stronger vorticity at its head. Next, this forward blob grows considerably, and a small patch of strong positive vorticity appears at the wall. By this time, the top of the structure is about 40 wall units from the wall, and a layer of negative vorticity has developed under it, separating it from the positive vorticity at the wall (see Fig. 5). It is not clear what is the origin of this negative vorticity, which was never observed at the wall itself. It most probably comes from the re-orientation of the streamwise or vertical vorticities which, in this late stage of evolution of the structure, are strongly present in the flow. It is clear, on the other hand, that the presence of this negative vorticity is important in inducing new positive vorticity at the wall (to maintain the no-slip condition), and that this effect is partly responsible for the appearance of the secondary wall vortex described above. Finally, that secondary vortex grows away from the wall and fuses with the tip of the stretching layer. At this moment, the tip separates from its parent structure, forming what appears to be the "embryo" of a new spot, and the cycle starts again (see Jiménez *et al.*, 1988).

The whole reproduction process is reminiscent of the instability process for 2-D linear Tollmien-Schlichting waves (see Betchov & Criminale, 1967). Basically, z-vorticity is created at the wall and diffuses into the main flow through viscosity, creating a strong wall vortex layer, with an average thickness of 10 wall units. If some part of this layer is lifted away from the wall, it is eventually carried forward by the flow (or, equivalently, by its own induced velocity). It is easy to see that, if the vortex layer is just lifted, leaving a "hole" of zero (weak) vorticity underneath, no extra vorticity is required to accommodate the no-slip condition. However, the resulting flow field develops an updraft at the forward end of the weak vorticity zone, and a stagnation point (in convecting axes) whose combined effect is to keep pumping new positive vorticity away from the wall along the separated shear layer. Eventually, this extra vorticity would end up inducing a secondary vortex of opposite sign at the wall (Fig. 12). This is basically the equilibrium configuration reached in two dimensions, but is never observed in 3-D. Before that happens, negative z-vorticity appears in the interior of the flow, probably through three dimensional effects which will be discussed in the next section, and this new layer overcomes the effect on the wall of the original structure, inducing the new positive wall vortex. The moment that a strong vortex pair in formed in this fashion, underneath the original structure, an updraft is created that carries part of the positive and negative vorticity into the upper part of the structure. The negative vorticity cuts the connection between the head and the base of old structure (through viscous annihilation), while the positive vorticity connects with the head of the old structure to form a new ejection.

Note that this mechanism, with minor variations, is the same one invoked for the ejections in two dimensional channels, involving the injection of vorticity into the flow along an stagnation point, and the generation of a spanwise secondary vortex pair at the wall, which produces a new updraft, and is responsible for the unsteady part of the ejection. This is essentially a two dimensional process, involving no streamwise vorticity, and is fundamentally different from the commonly quoted picture, which is dominated by self induction from hairpin vortices. We have shown that it is enough to explain many of the features observed in the simulation. It is nevertheless clear that longitudinal vorticity is present in the flow, especially away from the wall, and that some three dimensional mechanism has to be responsible for preventing the lateral spread of the shear layer into long spanwise bands. These effects will be discussed in the next section, in the context of a simplified model system.

A simplified three dimensional flow

The three dimensional structures described in the previous section are difficult to study due to the sheer volume of data involved, and to the wealth of phenomena present. Full numerical simulations of natural flows are essentially indistinguishable from experiments and, although the diagnostic tools are better developed in numerical flows than in physical ones, the full complication of turbulence is also present in the simulations, making the analysis of individual mechanisms very difficult. On the other hand, an advantage of numerical simulations is the possibility of studying simplified systems that cannot be conveniently set up experimentally, and that, hopefully, isolate particular aspects of a flow, while still retaining enough of the physics to be relevant to the original situation. While it is important to realise that these simplified systems are not the real thing, and that any extrapolation to the full flow has to be done with care, a lot of insight can be gained from them. This simplifying freedom of the numerical simulations is perhaps the characteristic that sets the ... more clearly apart from experiments.

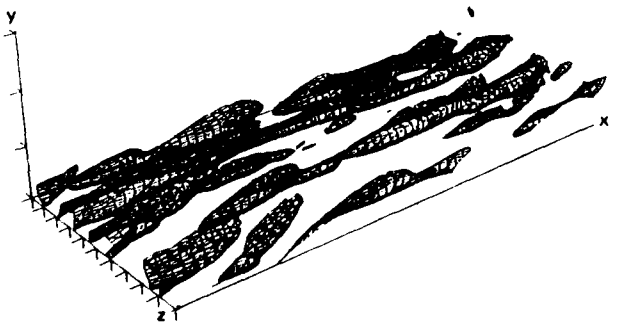

FIG. 6 Three dimensional representation of the vorticity isosurfaces extending away from the viscous sublayer. The isosurface represented is approximately 25% higher than the average wall value. (From Jiménez *et al.*, 1988).

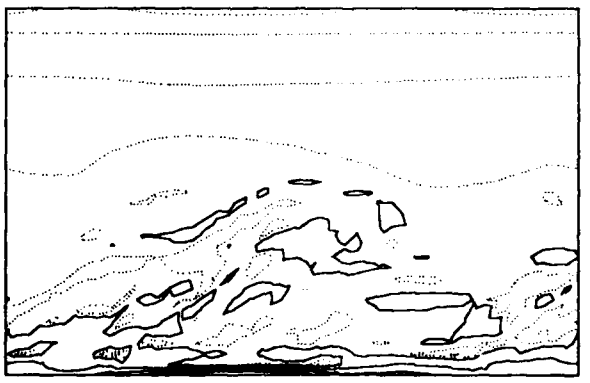

FIG. 7 Vorticity (ω_z) map of an x-y section of the $\pi \times \pi/8$ channel described in the text. Note the laminar two-dimensional flow near the top wall, and the turbulent character near the bottom one. Vorticity isolines, $\omega_z = -3, -2, -1, 0, 1, 4, 7, 10$. Dotted lines, zero or negative.

An extreme example is the two dimensional flow studied in the first part of this paper. It was shown that a simple oscillator exists in the wall region of that channel, driven by the coupling of the vorticity ejections from consecutive waves in an equilibrium wavetrain, and that this oscillator seems to "feed" the transition of that flow to two dimensional turbulence. It is tempting to extend this general model to the behaviour of the vorticity ejections in the wall layer in three dimensions, even if the detailed induction mechanisms might be different in that case. In the full flow, however, there are too many ejections and their positions and phases are too disorganised to try seriously to understand their behaviour.

With this in mind, we will attempt to define a "constrained" three dimensional channel that would still retain the ejections, but with less variation in their strengths and positions. The idea, as in the two dimensional flow, is to organise the flow field by making it periodic along its two homogeneous directions (stream and span-wise). If successful, this would convert the randomly appearing ejections into a uniform, doubly periodic, wave "array". The transversal, wall to wall, structure of the channel would not be constrained in any way. A rough count of "hot spots" in the sublayer of the KMM channel suggests a longitudinal wavelength of 1-3 channel half widths), equivalent to 200-500 wall units (Jiménez *et al.*, 1988), and a spanwise spacing of the order of 0.5 (100 wall units). This last number is consistent with the generally accepted spacing of longitudinal streaks in experimental sublayers.

Unfortunately, an early attempt to run a channel in a computational box of this size ($2\pi/5 \times \pi/8$, $Re_Q = 7000$), failed; a strong initial perturbation quickly decayed to laminar flow. The shortest computational box that we found to be able to maintain a turbulent flow for a long time, at this Re_Q, was a narrow one, with a longitudinal wavelength of π and a spanwise one of $\pi/8$. Actually, this channel decays to an asymmetric state, in which one on the walls is laminar, and the other one turbulent (Fig. 7). While this channel was not run for a very long time ($T \simeq 200$), and it is not sure that this is really its long time asymptotic state, another box ($2\pi \times \pi/8$), exhibiting the same odd behaviour, was run much longer ($T \simeq 1500$), without any signs of either the laminar wall turning turbulent, or the turbulent one turning laminar. The results reported in this section refer to the short box ($\pi \times \pi/8$) and assume that the asymmetric state is really a long time limit.

Fig. 8 shows the mean profiles for the basic statistical quantities for that channel. The asymmetry of the flow is evident, as is the fact that the upper wall is two-dimensional, since w' vanishes in that region. The two other components of the fluctuation velocity remain non-zero near the upper wall and, even if no detailed comparisons were made, that part of the flow looks similar to the two dimensional channels described in the first part of the paper. The profiles near the lower wall, on the other hand, look consistent with a fully turbulent flow. The average vorticity at that wall is $\overline{\omega}_z = 7.9$, corresponding to a wall shear velocity $u_\tau = 0.0336$, and to a wall Reynolds number $Re_\tau = u_\tau h/\nu = 235$. This stress is only 70% of the value recommended by Dean (1978) for a fully developed turbulent channel at the same Re_Q, but it is still more than twice higher than the stress observed for the two dimensional channels. Moreover, when the profiles near the lower wall are represented in wall units, using the actual u_τ, the results collapse reasonably well with the experimental results at similar Re_τ (Fig. 9). Also, most of the discrepancies between the simulation and the experiments, below $y^+ = 50$, are similar to those observed for the full channel in KMM. In particular, the large defect in w', which could be blamed on the narrow spanwise wavelength of the computational box, was also observed in that paper.

In summary, the basic statistical properties of the $\pi \times \pi/8$ channel, near the lower wall, correspond closely to those of natural flows for $y^+ < 50$. Above that range there are noticeable discrepancies and, in particular, the slope of the log layer is incorrect. This is probably related to the inability of the turbulent flow to penetrate all the way across the channel. In wall units, the width of the computational box is $z^+ = 92$ ($x^+ = 740$). While this spanwise wavelength might be appropriate to represent the streaky structure in the sublayer, it has never been observed experimentally outside it. The structures in the outer part of the layer are presumably larger (Cantwell, 1981) and, consequently, do not fit easily in the box. Thus, the narrow channel appears to be a suitable model for events in the sublayer, but not for the rest of the flow. The fact that, even under those conditions, the flow develops a turbulent structure, and is able to sustain a sublayer that looks similar to the experimental one, is significant in itself, and suggests that the sublayer is a largely self contained system, loosely coupled to the rest of the channel.

The 'hot spots' of high wall ω_z, described in the previous section, are also found here. There is usually one spot across the width of the box, and one or two in each longitudinal wavelength (Fig. 10). When they are quiescent, they move with a celerity $U_c \simeq 0.36$. This is lower than the celerity observed for the full channel in the previous section but, when expressed in wall units, both values become much closer; $U_c^+ \simeq 10.7$ for the narrow channel, and $U_c^+ \simeq 10.4$ for the wide one. Individual spots have a lifetime on the order of $T = 10$, during which they move about $x^+ = 1000$. After this time, they seem to elongate forward and "split", in a process that seems to be similar to the one described in the previous section for the full channel. Contrary to the observation in (Jiménez *et al.*, 1988) that, in the full channel, it was difficult to correlate the longitudinal vorticity it the wall with the presence of the spots, it is clear here that there is x-vorticity flanking active spots, especially those in the process of splitting (Fig. 10-c). The new spots created in this way move ahead, and to one side, of their parent structures, with the result that, when several spots are present in a single wavelength of the narrow channel, their arrangement looks staggered.

As described in the previous section, the spots are the roots of thin elongated layers of intense ω_z which protrude into the channel at shallow angles. The structure of these layers can be studied in Fig. 11 which shows the distribution of the three vorticity components in a sequence of transversal sections of one of them. As in the previous figure, these sections include two identical spanwise wavelengths, to aid in the interpretations of the maps.

Two features are apparent in the ω_z maps: first, the presence of a well defined vortex layer near the wall, with intensities that are an order of magnitude larger than those in the rest of the flow, and the character of the shear layers as patches of the wall layer that have been lifted away, leaving behind an empty "trench", in which the wall shear is much weaker and, in fact, comparable to the values typical of the laminar channel. There is also negative ω_z in the flow, but it only appears well into the channel, and it does not seem to originate from the wall. As pointed before, it most probably comes from the secondary rotation of ω_x or ω_y, once the flow becomes complex in that region.

The ω_y map is dominated by vertical "walls" that connect the strong ω_z and ω_x features to the wall layer. This has to be so. The only source of circulation is the viscous interaction at the wall, and all the strong vortices, of whatever sign and direction, eventually have to be connected to that source. Small, localised regions of intense vorticity can be generated by stretching, but any appreciably strong circulation can only come from a reasonably large piece of the wall layer that has been lifted and deformed. The ω_y "sidewalls" are the connections of these pieces to the parts of the wall layer that still remain "in place".

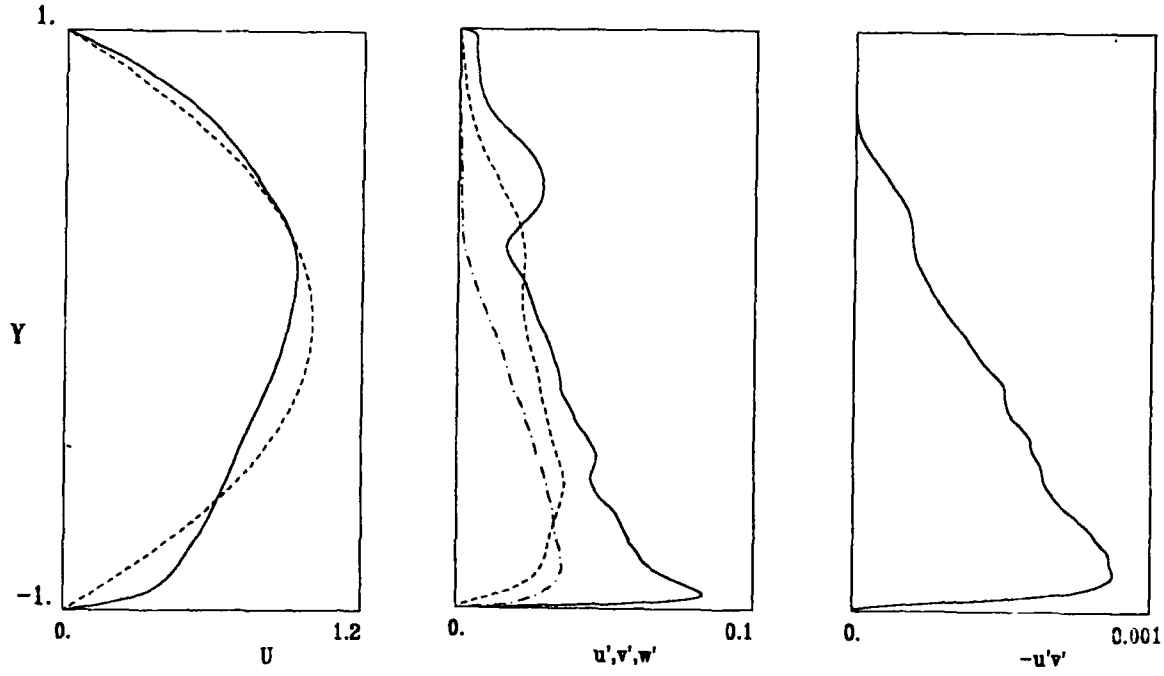

FIG. 8 Profiles for the statistical properties of the $\pi \times \pi/8$ channel. **Left**, average velocity and laminar profile with the same mass flux. **Centre**, turbulent r.m.s. intensities. Solid line: u'; dashed: v'; dot-dashed: w'. **Right**, Reynolds stress.

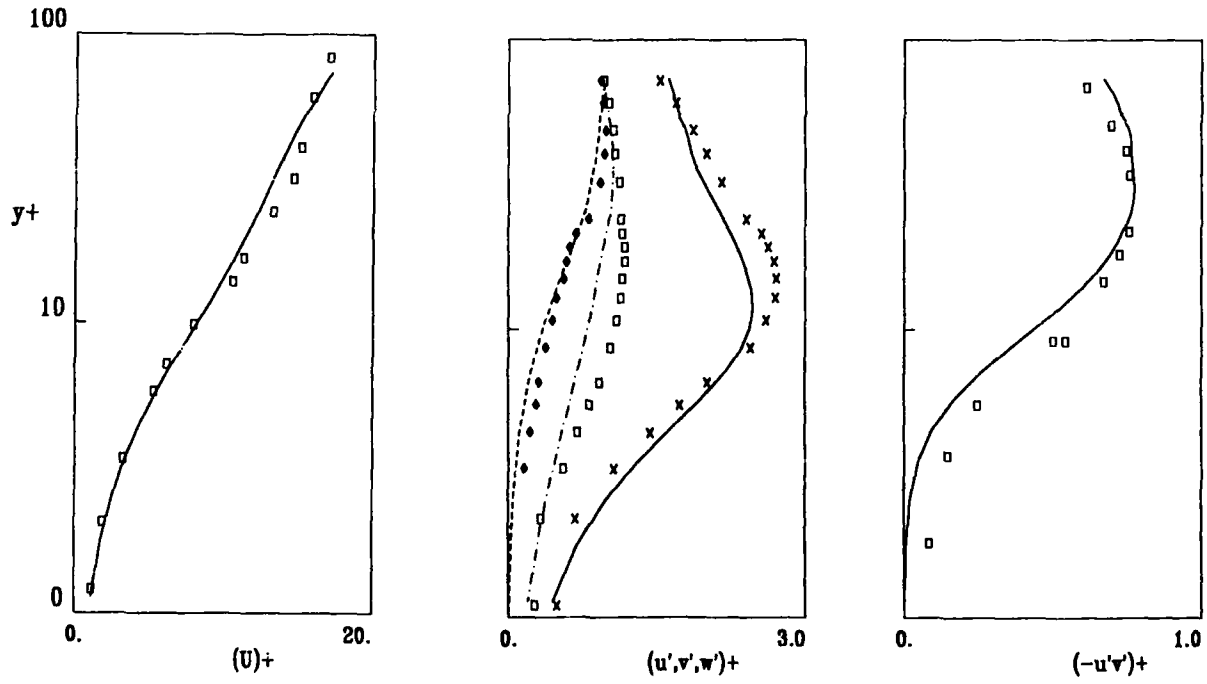

FIG. 9 Profiles for the statistical properties at the lower wall region of the $\pi \times \pi/8$ channel, expressed in wall units. Symbols are experimental data, re-scaled to a 6% higher u_τ, as in KMM. **Left and right**, data from Eckelmann (1974), at $Re_\tau = 208$. **Centre**, turbulent intensities from Kreplin & Eckelmann (1979), $Re_\tau = 194$, For the present run, $Re_\tau = 235$.

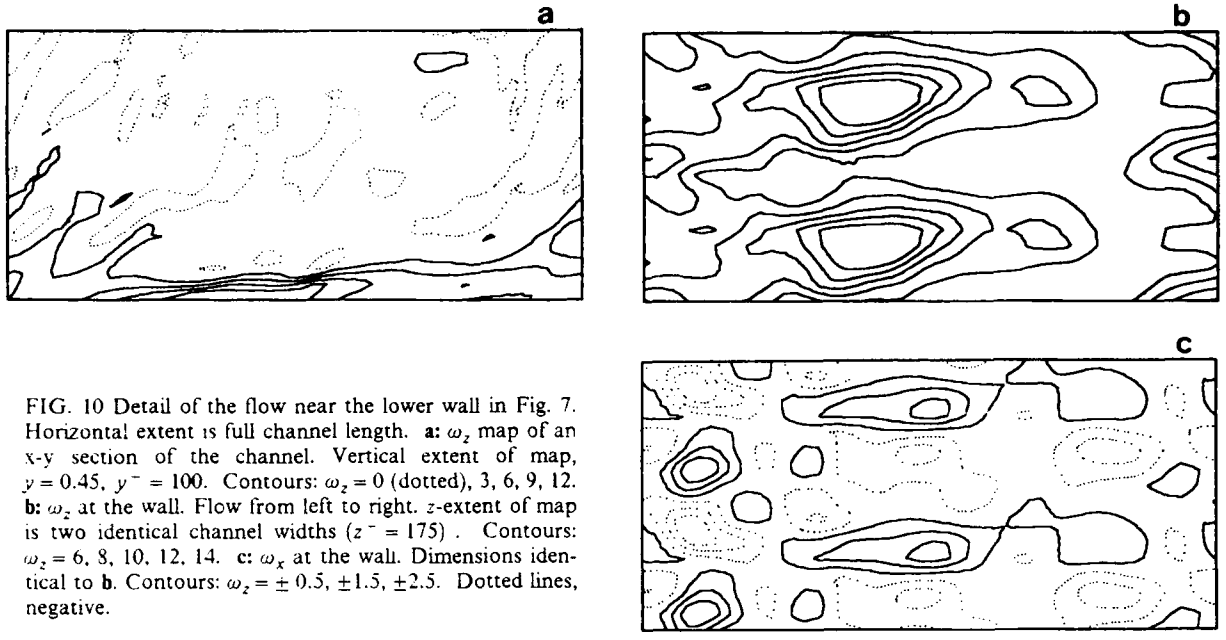

FIG. 10 Detail of the flow near the lower wall in Fig. 7. Horizontal extent is full channel length. **a:** ω_z map of an x-y section of the channel. Vertical extent of map, $y = 0.45$, $y^- = 100$. Contours: $\omega_z = 0$ (dotted), 3, 6, 9, 12. **b:** ω_z at the wall. Flow from left to right. z-extent of map is two identical channel widths ($z^- = 175$). Contours: $\omega_z = 6$, 8, 10, 12, 14. **c:** ω_x at the wall. Dimensions identical to **b**. Contours: $\omega_z = \pm 0.5, \pm 1.5, \pm 2.5$. Dotted lines, negative.

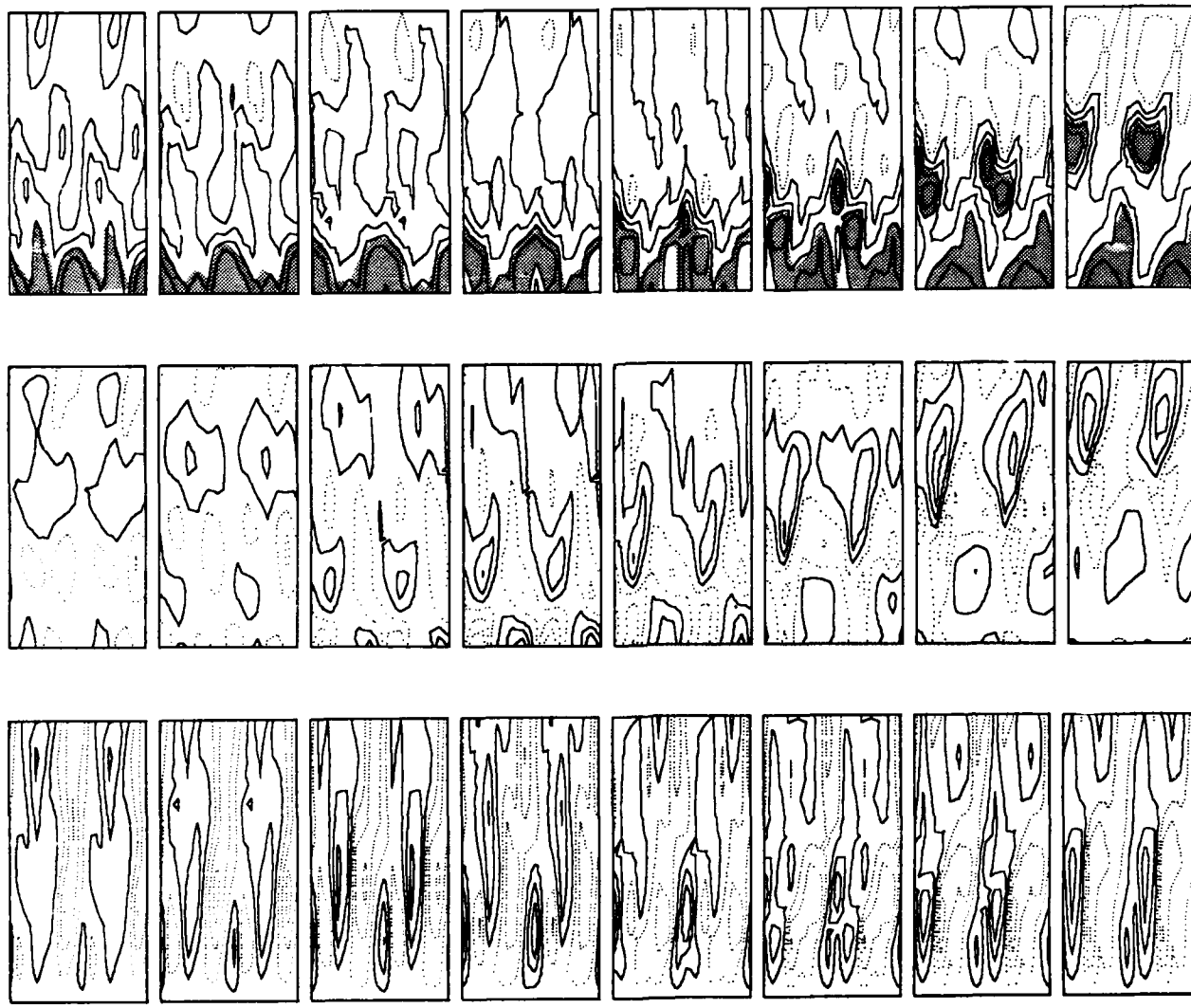

FIG. 11 Transversal z-y sections of flow near lower wall. Horizontal extent is two channel widths; vertical, $y^+ = 40$. Streamwise distance between sections, $x^+ = 23$, left to right. Set corresponds to first quarter of Fig. 9. **Top:** ω_z. Contours: 0 (dotted), 2, 4, 6, 8. Shaded area, > 6. **Middle and bottom:** ω_x and ω_y. Contours: $\omega_z = \pm 0.5, \pm 1.5, \pm 2.5$. Dotted lines, negative.

The map of longitudinal vorticity, ω_x, is also well organised. There are periodic arrays of longitudinal vortices of alternating sign that appear at the wall and then lift, following roughly the direction of the ω_z layers. They are also in phase with the spanwise modulation of the thickness of the wall ω_z layer, and tend to be located at the points where the slope of this variation is maximum. In fact, the effect of this array of x-vortices is to produce an up-draft in those locations in which the ω_z layer separates from the wall (the "trenches"), and a down-draft where it stays attached (the "ridges"). Also, since the longitudinal velocity is zero at the wall and since $\omega_z = \partial U/\partial y$ at that point, the trenches correspond exactly to the low velocity streaks of the experimenters.

An obvious feature of the maps in Fig 11 is that there are several vortex systems stacked on top of one another. This is most evident in ω_x, in which three different levels can be easily distinguished: a strong vortex pair that runs diagonally from bottom-left to top-right, a younger system that originates near the centre section and lifts to the right, and an older one that rides on top of the other two, and leaves the field of view near the middle of the picture. The same layered structure can be traced in the ω_z map, with the ω_z features interleaved in between the ω_x layers. The most striking characteristic of this arrangement is that the vertical stacking is alternating; positive x-vortices overlay negative ones, and ω_z ridges overlay trenches. When other structures are observed in other frames of the simulation, there are many variations and complications, but the layered structure and the sign alternation seems to be a most common feature. The angle that the structures form with the wall is about 20°.

Discussion

We have discussed in the previous sections a variety of phenomena related to the behaviour of the viscous sublayer of turbulent channel flows. We will try here to discuss the relation, if any, among them and to draw a series of cartoons of the possible sequence of events in the sublayer of natural turbulent channels, as suggested by the partial views that we have presented up to now. In essence, we will try to reconstruct the "elephant" of the classical tale and, as such, our picture will probably be erroneous or incomplete. Much of the evidence will come from "elephants in captivity", such as the two dimensional or the spanwise periodic channel. Our hope is that some of the features seen in those simplified flows correspond to partial aspects of real structures, and that we will be able to choose the right ones. The experience with the transition to turbulence in the two dimensional channel is encouraging. There, at least, the simple limit cycle of the periodic wavetrains seems to be still an important dynamical feature of the "wilder" turbulent flow. Still, it should be remembered that serious hunters claim that an elephant in a zoo has nothing to do with real beast in the wild.

The basic mechanism of ejection in two dimensions seems to be clear (Fig. 12). if, for any reason, a patch in the wall vortex layer breaks away from the wall, the vertical velocities induced at the edges of the resulting spanwise "trench" will, first, tend to rotate it into a little forward rising ramp, and, then, to stretch the resulting shear layer forward, forming a permanent path along which vorticity can bleed from the wall into the outside flow, along the unstable direction of a saddle point that forms at its base. The process eventually stops when the extra positive vorticity in the separated layer induces a secondary negative vortex at the wall. This vortex widens the trench, weakening the saddle until the vorticity outflow stops. In fact, the result of this process is the creation of a new saddle ahead of the negative vortex that regenerates the ejection at a new location.

The final stage of this process, in a simplified periodic situation, is the nonlinear wavetrain that was discussed in the first part of the paper. In more complicated situations, it leads to the unsteady limit cycle or to the chaotic flows also discussed there. Since the only prerequisite for this process is a streamwise variation of the strength of ω_z in the wall layer, and since we have shown that three dimensional channels have strong variations of this kind (the "hot spots"), it is clear that this process also has to be active in three dimensions. In fact, the observation of strong separated ω_z layers confirms that predictions. However, both the hot spots and the layers have only a finite spanwise extent, and the general disposition of the wall layer should look, from observations, something like Fig. 13. This three dimensional arrangement has important consequences since, immediately, all the other components of vorticity appear in the flow. The most obvious is ω_y, which must appear in the form of the vortex "sidewalls", linking the sides of the lifted ramps to the wall layer where they originated. These ω_y walls were clearly observed in the narrow channel, and were also reported for the wide channel in (Jiménez *et al.*, 1988). Also, as the vortex ramps are carried forward by the effect of the ω_z wall layer, their sides, which are rooted to the wall, and which do not move, are stretched, forming two counter-rotating ω_x vortices (Fig. 14). This is the classical view of the formations of "hairpins".

It is important to realise that, although a single hairpin, formed in this fashion, will tend to lift away from the wall, an array of them, periodic across the span, will not. In fact, such an array is equivalent to an equidistant array of alternating vortices, which is an equilibrium arrangement that will not move at all. The x-vortices observed in the periodic channel form, at least near the wall, a roughly equidistant array, with each negative vortex lying approximately at the mid point between the two neighbouring positive ones (Fig. 11). This might be an artefact of the periodicity imposed to the simulation, but that periodicity was included to model a very strong, experimentally recognised period of natural flows, and therefore, probably represents an important part of the behaviour of the unconstrained channel. This is also suggested by the similarity of the dimensionless statistical profiles of the two sublayers. If this is so, the only mechanism available to lift the hairpins from the wall is the same ω_z induction discussed in two dimensions.

The x-vortices, however, have several important effects. The first one is shown in Fig. 15, and is to buckle inwards the ω_y "sidewalls" that form the sides of the ramps. This is equivalent to creating negative z-vorticity underneath the ramps, and is the most likely origin for the negative vortex sheet that was observed to form, away from the wall, both in the narrow and in the wide three dimensional channels. This is a faster process than the induction of negative vorticity at the wall, and will tend to shield the effect of the rising ramp faster than the two dimensional process. This might be one of the reasons why the characteristic wavelengths and dimensions are shorter in three dimensions than in two.

A secondary effect, that does not really belong to the sublayer, is the influence of the ω_y "sidewalls" on the hairpins that ride on their top. It is easy to see that the direction of the y-vorticity is such as to draw the front part of the hairpins closer together, so that even a periodic array would rise under its self induction. Note that this effect is only important away from the wall, once the y-vortices have had time rotate the longitudinal pairs. In fact, it seems clear from many observations, that, above $y^+ = 50$-100, hairpin self induction in indeed important, and that the flow is much more complicated, in that region, that any of the models described here.

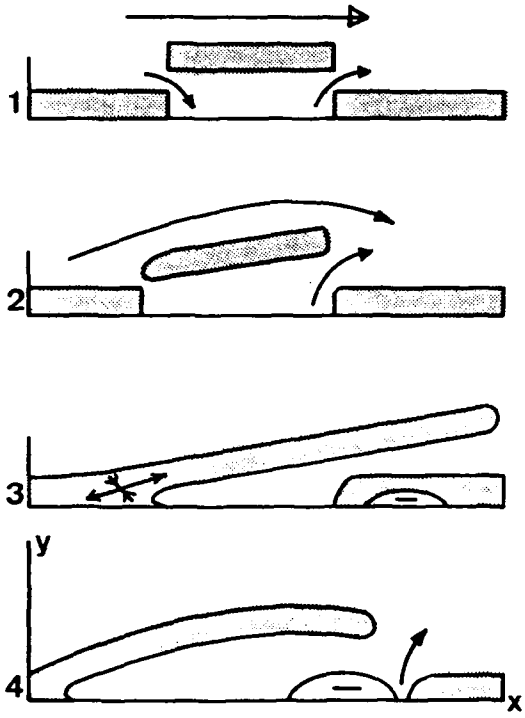

FIG. 12 The two dimensional ejection mechanism, including saturation through secondary production of negative wall vorticity. Time goes from top to bottom.

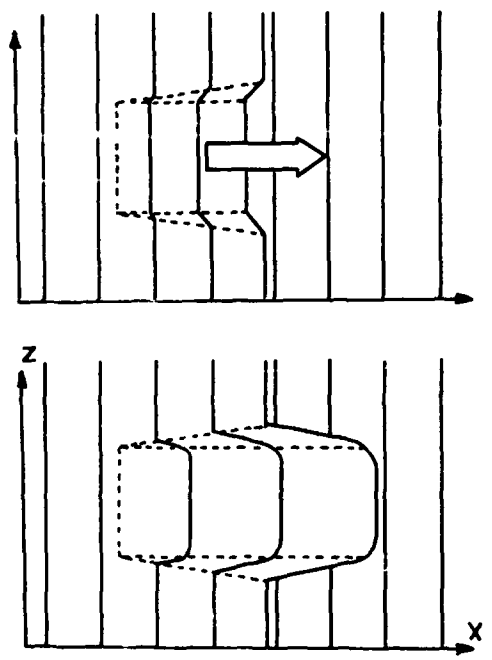

FIG. 14 As a ramp is stretched by ω_z induction, it creates a longitudinal vortex pair.

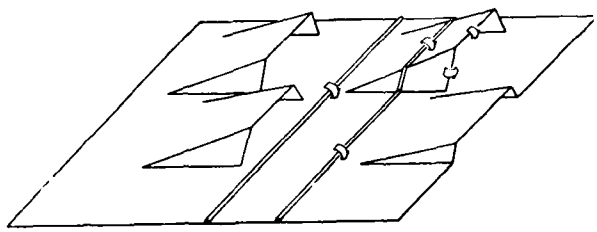

FIG. 13 In three dimensions, vortex layers turn into "ramps" with a finite spanwise extent, connected to the wall layer by vertical "sidewalls". Flow is from left to right.

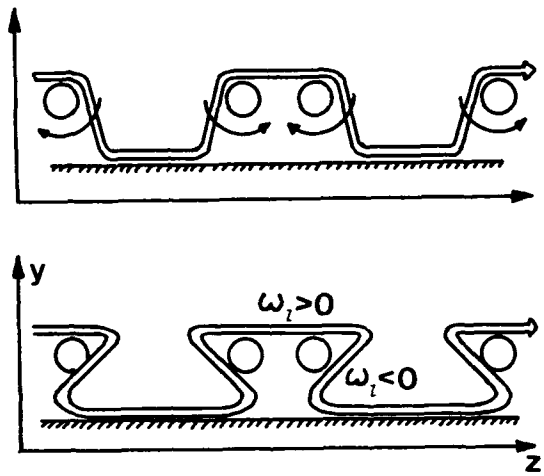

FIG. 15 A uniform array of vortex pairs will not rise on its own, but it will deform the vertical "sidewalls" of the ramps carrying it, creating negative ω_z vorticity underneath it.

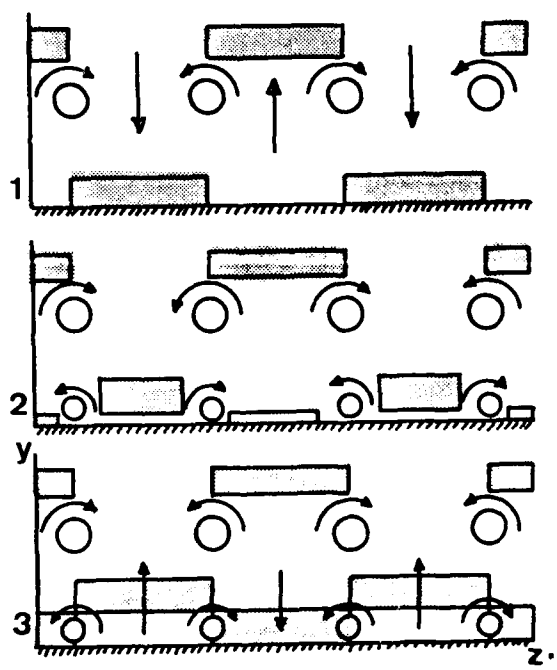

FIG. 16 A raised longitudinal vortex array will induce a array of opposite sign at the wall which, in turn, will rearrange ω_z vorticity, and restart the cycle at a different position.

The most important effect of x-vorticity is different. Once a longitudinal vortex array is created, in any way, and lifted away from the wall, it induces a secondary array, of opposite sign, at the wall to maintain the no-slip condition. These secondary arrays are clearly seen in the cross-sections of Fig.11, and are responsible for the staggered stacking in that picture. This secondary array is, as explained above, unable to rise on its own, but it will immediately begin to reorganise the ω_x vorticity at the wall layer. When it is created, the sign of the induced array is such as to induce an updraft at the places where the wall layer is attached, and a downdraft at those places where it is not (Fig. 16). The updrafts will then initiate the detachment of the wall layer, in those places where it was attached, while the downdrafts will tend to "heal" the trenches left by the previous generation of ejections. In this way, trenches tend to appear below ridges, and viceversa, and the cycle begins again, although staggered half a spanwise wavelength away from the previous one. This staggering was clearly observed in the narrow channel, and has been suggested before by other investigators. Moreover, this mechanism offers a first indication of how spanwise periodicity is established and maintained. In fact, a single longitudinal vortex pair, created alongside a trench by secondary induction from a previous generation ramp, will create enough of an updraft on its outside "wings", and enough of a downdraft on its centre, to heal its trench and to initiate the formation of two new ones at its sides, thus providing a lateral contamination mechanism that might eventually lead to a spanwise periodicity.

In summary, we have proposed a cyclical mechanism involving the interplay of the three vorticity components, by which trenches in the ω_x wall layer give rise to ejection ramps, which in turn generate longitudinal vortex pairs, which induce secondary longitudinal pairs at the wall, which initiate new trenches and re-start the cycle. The mechanism explains many details of the observations that we have reported along this paper regarding the sublayer in several channels flows, and offers an interface to the more complicated phenomena that appear to dominate the outer part of the turbulent boundary layer. There are however many details that are left out of this model, including, very especially, the possibility of making quantitative predictions of the flow, but we believe that the present method of studying simplified model cases that isolate particular aspects of the flow offer the best hope at filling in those details. We are continuing work in that direction.

References

Betchov,R. & Criminale,W. (1967) *Stability of parallel flows*, Academic Press, Ch. 11.

Cantwell,B.J. (1981) Organised motion in turbulent flow, *Ann. Rev. Fluid Mech.*, **13**, 457-515.

Dean,R.B. (1978) Reynolds number dependence of the skin friction and other bulk variables in two-dimensional rectangular duct flows, *Trans. ASME I: J. Fluids Engng*, **100**, 215-223.

Eckelmann,H. (1974) The structure of the viscous sublayer and the adjacent wall region in a turbulent channel flow, *J. Fluid Mech.*, **65**, 439-

Herbert,T. (1976) Periodic secondary motions in a plane channel, in *Proc. 5th. Int. Conf. on Numerical Methods in Fluid Dynamics*, edited by A.I. Van de Vooren and P.J.Zandbergen, pp. 235-240, Springer, Berlin.

Jimenez,J. (1987) Bifurcations and bursting in two dimensional Poiseuille flow, *Phys. Fluids*, **30**, 3644-3646.

Jiménez,J. (1988a) Bifurcations and turbulence in plane Poiseuille flow, *Proc. Zaric Memorial Int. Sem. on Wall Turbulence*, Dubrovnic, Yugoslavia, May 16-20.

Jiménez,J. (1988b) Chaotic behaviour in two-dimensional Poiseuille flow, *to appear*.

Jiménez,J., Moin,R., Moser,R. and Keefe,L. (1988) Ejection mechanisms in the sublayer of a turbulent channel, *Phys. Fluids*, **31**, 1311-1313.

Kim,J., Moin,P. and Moser,R. (1987) Turbulence statistics in fully developed channel flow at low Reynolds number, *J.Fluid Mech.*, **177**, 133-166

Kreplin,H. and Eckelmann,H. (1979) Behaviour of the three fluctuating velocity components in the wall region of a turbulent channel flow, *Phys. Fluids*, **22**, 1233-

Orszag,S.A. and Patera,A.T. (1983) Secondary instability of wall bounded shear flows, *J. Fluid Mech.*, **128**, 347-385.

Rozhdestvensky,B.L. and Simakin,I.N. (1984) Secondary flows in a plane channel: their relationship and comparison with turbulent flows, *J. Fluid Mech.*, **147**, 261-

Zahn,J.P., Toomre,J., Spiegel,E.A. and Gough,D.O. (1974) Nonlinear cellular motions in Poiseuille channel flow, *J. Fluid Mech.*, **64**, 319-345

Acknowledgements.

This work was supported in part by a grant of computer time at the IBM-3090 of the CIEMAT Centre at Madrid, and by the Joint Spain-US Committee for Scientific and Technological Cooperation, under contract CCA-8510/057. The narrow channel simulation and the analysis of the wide channel were done during two separate stays at the Centre for Turbulence Research, at Stanford University and NASA Ames, whose support is gratefully acknowledged. The rest of the work was supported by the IBM Madrid Scientific Centre. I am especially grateful to P.Moin, R.Moser, J.Kim and L.Keefe, at the CTR, for providing the raw data for the wide channel, as well as the code for running the 3-D narrow channel. I am also indebted to all of them for many stimulating discussions.